Functional Delivery of siRNA in Mice Using Dendriworms

Amit Agrawal,[†] Dal-Hee Min,[†] Neetu Singh,[†] Haihao Zhu,[‡] Alona Birjiniuk,[†] Geoffrey von Maltzahn,[†] Todd J. Harris,[†] Deyin Xing,[§] Stephen D. Woolfenden,[‡,§] Phillip A. Sharp,[§] Alain Charest,[‡,§] and Sangeeta Bhatia[†,⊥,¶,*]

[†]Harvard—MIT Division of Health Sciences and Technology, MIT, Cambridge, Massachusetts 02139, [‡]Tufts University School of Medicine, Tufts Medical Center, 800 Washington Street, Boston, Massachusetts 02111, [§]Department of Biology, MIT, Cambridge, Massachusetts 02139, [⊥]Electrical Engineering and Computer Science, Massachusetts Institute of Technology, Cambridge, Massachusetts 02139, and [¶]Division of Medicine, Brigham and Women's Hospital, Boston, Massachusetts 02115

ABSTRACT Small interfering RNAs (siRNAs) mediate cleavage of specific, complementary mRNA sequences and thus regulate gene expression. Not surprisingly, their use for treatment of diseases that are rooted in aberrant gene expression, such as cancer, has become a paradigm that has gained wide interest. Here, we report the development of dendrimer-conjugated magnetofluorescent nanoworms that we call "dendriworms" as a modular platform for siRNA delivery *in vivo*. This platform maximizes endosomal escape to robustly produce protein target knockdown *in vivo*, and is tolerated well in mouse brain. We demonstrate that siRNA-carrying dendriworms can be readily internalized by cells and enable endosomal escape across a wide range of loading doses, whereas dendrimers or nanoworms alone are inefficient. Further, we show that dendriworms carrying siRNA against the epidermal growth factor receptor (EGFR) reduce protein levels of EGFR in human glioblastoma cells by 70—80%, 2.5-fold more efficiently than commercial cationic lipids. Dendriworms were well-tolerated after 7-days of convection-enhanced delivery to the mouse brain and in an EGFR-driven transgenic model of glioblastoma, anti-EGFR dendriworms led to specific and significant suppression of EGFR expression. Collectively, these data establish dendriworms as a multimodal platform that enables fluorescent tracking of siRNA delivery *in vivo*, cellular entry, endosomal escape, and knockdown of target proteins.

KEYWORDS: dendrimer · siRNA · nanoparticle · EGFR · glioblastoma

Small interfering RNAs (siRNAs) are 21—23 nucleotide double strand nucleic acid molecules that assemble into specific complexes in mammalian cells to mediate cleavage of complementary mRNA sequences and thus regulate gene expression.[1] As a result, their use as a tool for target validation, genetic studies, and for therapy of diseases that are rooted in aberrant gene expression, such as cancer,[2,3] has become increasingly popular.[4—9] However, unlike small molecule drugs that are often hydrophobic and easily cross the cell membrane, siRNAs are negatively charged and cannot freely traffic to the cytoplasm of the target cells. Thus, delivery of intact, functional siRNAs into the cytoplasm of target cells *in vivo* is a major impediment to realizing the potential of siRNA-based protein modulation in disease.

To date, several formulations that deliver siRNAs into cells *in vitro* and *in vivo* have been reported. siRNA backbone or end-groups modifications that impart siRNA serum stability and improve cell membrane penetration have been used successfully to knockdown genes *in vivo*.[10,11] Protamine-antibody fusions have also been used to successfully transfect HIV infected T cells.[12] Lipid-based and lipid-derived nanoparticles that carry siRNAs either in their core or *via* covalent attachment have been reported to have significant efficacy *in vivo* and *in vitro*.[13—15] However, these formulations do not contain imaging agents that can be traced *in vivo* to assess the location of the carrier and siRNAs. To address this issue, many research groups have used quantum dots,[16] magnetic[17] and gold nanoparticles[18,19] as well as carbon nanotubes[20] and enabled successful siRNA/ antisense delivery *in vitro*,[16,19,20] with a few reports on *in vivo* imaging of these nanoparticles.[17] However, in these reports (where inorganic nanoparticles are used), covalent coupling of siRNAs is used to formulate the nanoparticles which makes rapid testing of various siRNA formulations a cumbersome and iterative process. Thus, to screen for maximum efficacy, it is desirable to have a simple formulation that affords use of different siRNAs in a variety of dosages. Finally, most nanoparticle-based siRNA delivery reports use a model gene to demonstrate knockdown in non-native tissues of animals, which may not be equivalent to a native disease model. Overall, while the above reports highlight significant advances in siRNA delivery, there is a need for a versatile siRNA delivery vehicle

*Address correspondence to sbhatia@mit.edu.

Received for review March 1, 2009 and accepted August 4, 2009.

Published online August 12, 2009.
10.1021/nn900201e CCC: $40.75

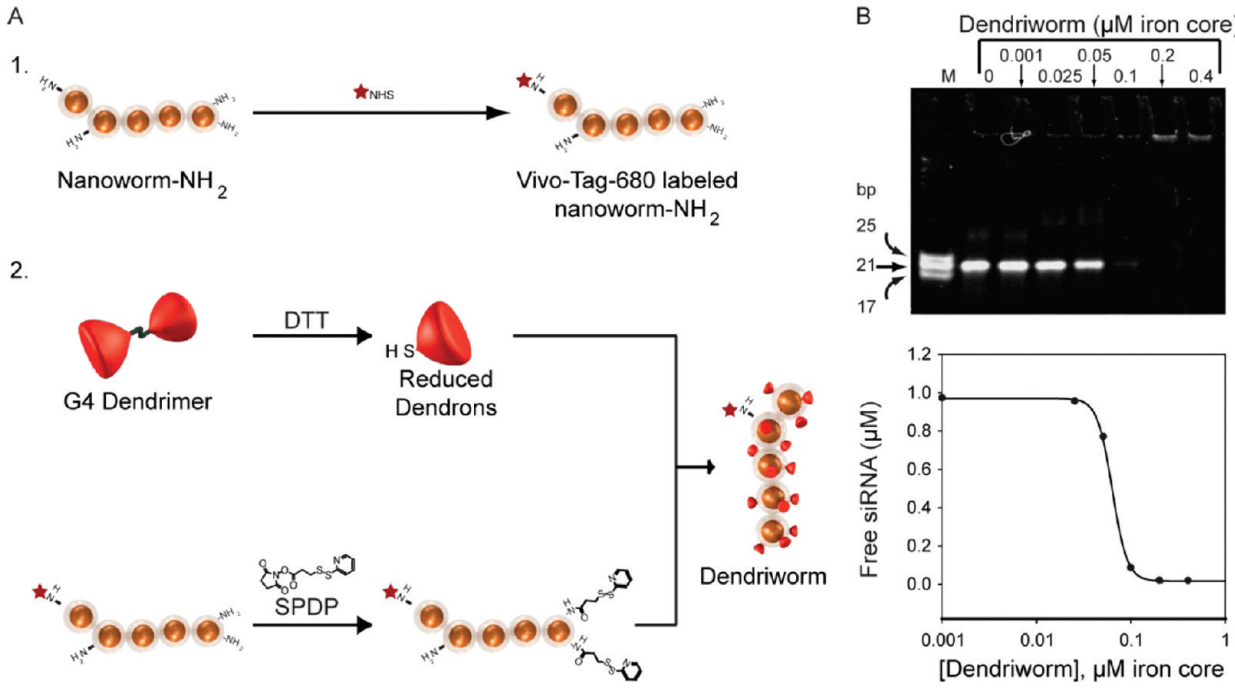

Figure 1. Synthesis and characterization of dendriworms: (A) synthesis scheme; (B) siRNA binding characteristics. Dendriworm and siRNAs were allowed to bind in varying ratios and run on a gel. Strong binding between the dendriworm and siRNA at roughly 1:10 ratio (measured using iron core concentration) prevents siRNAs from entering the gel.

that is nontoxic, allows flexible siRNA loading, and can be used *in vivo* in a native disease model.

In this work we report synthesis, systematic *in vitro* evaluation, and *in vivo* application of polyvalent, dendrimer-bearing, magnetic nanoparticles (dendriworm) as a carrier for siRNA delivery in a transgenic murine model of glioblastoma. The construct overcomes issues highlighted above. First, dendriworms contain magnetic core and are labeled fluorescently to enable imaging in a variety of formats. Second, we establish that dendriworms promote cytosolic release of the endocytosed cargo more efficiently than their components, resulting in efficient delivery of siRNA to the cell cytoplasm over a wide range of loading doses. Finally, noncovalent attachment of siRNA affords dendriworms the ability to retain flexibility in siRNA loading without reformulation and enabled a smooth transition to *in vivo* applications where dendriworms were well tolerated after 7 days of convection-assisted delivery in the CNS and resulted in knockdown of EGFRvIII in a transgenic model of glioblastoma. In the future, this multimodal platform may be further enhanced to include affinity ligands for targeting to particular cells of interest.

RESULTS AND DISCUSSION

Polyamidoamine (PAMAM) dendrimers are cationic polymers that have been extensively evaluated as candidates for gene delivery.[21] Dendrimers are branched, multivalent macromolecules that were first reported nearly two decades ago.[22,23] Dendrimers can be synthesized to have neutral, cationic,[22] or anionic[24] groups in a cascade polymer form, enabling facile regulation of a number of functional groups, size, and charge. Multiple surface groups on dendrimers can be linked with polymers,[25] amino acids,[26] tissue targeting moieties,[27,28] drugs,[29−31] nucleic acid molecules,[32] or imaging agents[33] to modulate properties of the dendrimer-based drug or imaging agent carriers.[34,35]

Synthesis and Characterization of Dendriworms. While dendrimers have been used for delivery of genes[21,36] and antisense oligonucleotides,[37,38] delivery of siRNA with dendrimers has been challenging[37] and only poor efficiencies have been reported.[38,39] A recent report demonstrates use of generation 7 PAMAM dendrimers for siRNA delivery,[40] but most efforts using lower generation dendrimers for siRNA delivery have been unsuccessful[37,38] and it has been shown that lower generation dendrimers are poor at forming uniform, stable particles with siRNAs.[41] In a recent report, generation 6 polylysine dendrimers were also found to be inefficient for delivery of siRNAs.[39] Since dendrimers buffer the endosomes *via* their tertiary and secondary amines, we hypothesized that polyvalent conjugation of lower generation dendrimers onto an elongated magnetic nanoparticle host could generate a construct that would induce high proton sponge effect and enable efficient endosomal escape of siRNAs. Use of lower generation dendrimers may also diminish the likelihood of immune system activation and inflammatory response associated with the use of higher generation dendrimers.[42] Also, to encourage further *in vivo* use, we chose a magnetic nanoparticle scaffold that could be conjugated to fluorophores or imaged *via* magnetic resonance imaging.

The synthesis of dendrimer-conjugated magnetic nanoworms (dendriworms) is shown in Figure 1A. First,

generation 4, cystamine core PAMAM dendrimers were reduced in 0.5 M dithiothreitol (DTT), and excess DTT was removed using a G25 chromatography column. Next, amine-modified, cross-linked iron oxide nanoworms, labeled with near-infrared fluorochromes (VivoTag 680, Visen Medical, Inc.), were prepared as detailed in the Experimental Section. Finally, reduced dendrons and nanoworms were conjugated using the heterobifuctional linker *N*-succinimidyl 3-(2-pyridyldithio)-propionate, which links amine groups on the nanoparticle with the central thiols on reduced dendrons (Figure 1A; see Experimental Section for details). The resulting dendriworms were separated from free dendrons by filtering several times using either 100,000 molecular weight cutoff filter (Amicon Ultra, Millipore Corp.), magnetic separation column (MACS, Miltenyi Biotech), or G50 chromatography columns. Dendriworms were stored at 4 °C protected from light and were stable for at least 6 months. Net charge on dendriworms was found to be between 16−24 mV (zeta-potential measurement in 1× PBS) and the average hydrodynamic diameter was found to be between 80 and 110 nm (dynamic light scattering measurements in 1× PBS, Zetasizer Nano, Malvern, Inc.). In the transmission electron micrograph, the particles were found to retain a worm-shape, where multiple 5−8 nm iron oxide cores were lined in a series (data not shown).[43] The number of dendrons per dendriworm was found to be 45−50 using fluorescamine and ninhydrin tests (assuming there are approximately 7 iron cores per dendriworm). Further, using UV−vis absorbance measurements, the number of VivoTag on each dendriworm was found to be between 1 and 5. A key feature of the dendriworms is that dendrons are conjugated via a reducible linker (SPDP) to the nanoparticle surface. This may allow removal of dendrons from the nanoparticle surface in the reducing intracellular environment, resulting in improved siRNA delivery and diffusion inside cells. Variations of magnetic-core particles were also generated using other polymers [polyethyleneimine, myristic acid] and generations 3−6 of PAMAM dendrimers. However, these particles were found to be ineffective for gene silencing either due to a lack of colloidal stability or due to poor siRNA delivery efficiency and were therefore not pursued further (data not shown).

Next, the binding affinity of siRNA and dendriworms was tested by incubating varying amounts of dendriworms (10−400 nM iron core) with 1 μM of siRNA for 10 min at room temperature and measuring the amount of siRNA left unbound. The mixture was run on a 15% TBE gel (BioRad Laboratories) at 80 mV for 1 h and siRNAs in the gel were stained with SYBR Gold (Invitrogen Inc., Carlsbad, CA) Figure 1B. Because dendriworms are large and positively charged, they do not electrophorese into the gel toward the cathode and are washed from the top of the gel during the 1 h run. Further, dendriworms bound to siRNAs remain positively charged (zeta-potential measurements), causing siRNA binding to dendriworms to retard siRNA movement into the gel. At 50 nM dendriworm (iron core concn.), some loss in siRNA band (21 bp) intensity was observed and at 100 nM dendriworm (iron core concn.), nearly complete siRNA retardation was seen. Thus, roughly 9−10 siRNA molecules are bound to each iron core in dendriworm. This implies roughly 50 siRNA molecules loaded on each dendriworm (there are roughly 7 iron cores per dendriworm). To maintain consistency, amounts of dendriworm and nanoworm are expressed in iron core concentration in the rest of the manuscript. The stability of the siRNA-dendriworm nanoparticle was assessed in fetal bovine serum (FBS) and artificial cerebrospinal fluid (ACSF) by gel electrophoresis and dynamic light scattering. To visualize the residual bound siRNA, 1% SDS was used to release the siRNA prior to electrophoresis. In ACSF the nanoparticle and the bound siRNA remained stable for up to 6 h (Supporting Information, Figure S1); however, the siRNA showed lower stability in serum (data not shown).

Dendriworms Enable Efficient Release of Cargo into the Cell Cytosol. Cationic polymers adhere to the negatively charged moieties on the cell membrane and may be taken up *via* fluid phase endocytosis or *via* receptor mediated endocytosis.[44] As a result, a cargo that is only active in the cell cytoplasm and is delivered using cationic polymers or cationic nanoparticles needs to escape the endosomes. To test our hypothesis that conjugating multiple cationic dendrimers on a nanoworm scaffold would enhance the proton sponge effect, leading to better cytosolic release of cargos, we evaluated the efficiency of dendriworm endosomal escape compared to free dendrimers. To assess endosomal escape, we codelivered excess of a membrane impermeable dye (Calcein at 0.25 mM) along with the siRNA delivery agent (dendrimer, unmodified nanoworms and dendriworms) coupled with siRNAs and counted the fraction of cells with endosomal escape as indicated by diffuse cytoplasmic distribution of the dye.[45,46]

The results of these endosomal escape experiments are shown in Figure 2. Aminated nanoworms (200 nM iron core), dendrimer (30 μM), or dendriworm (200 nM iron core) were incubated with 100 nM siRNA in serum-free cell culture medium containing excess of Calcein for 10 min at room temperature and transferred over the cells. The cells were kept at 37 °C and 5% CO_2 environment for 1 h and imaged using an inverted microscope. In the presence of Calcein alone, punctate cytoplasmic distribution of dye was consistent with the endosomal uptake. Some degree of endosomal release as judged by diffuse cytoplasmic distribution was seen with aminated nanoworms. Significantly more endosomal escape was seen with both dendrimers and dendriworms, although the extent of endosomal escape was much greater with dendriworms. Endosomal escape is

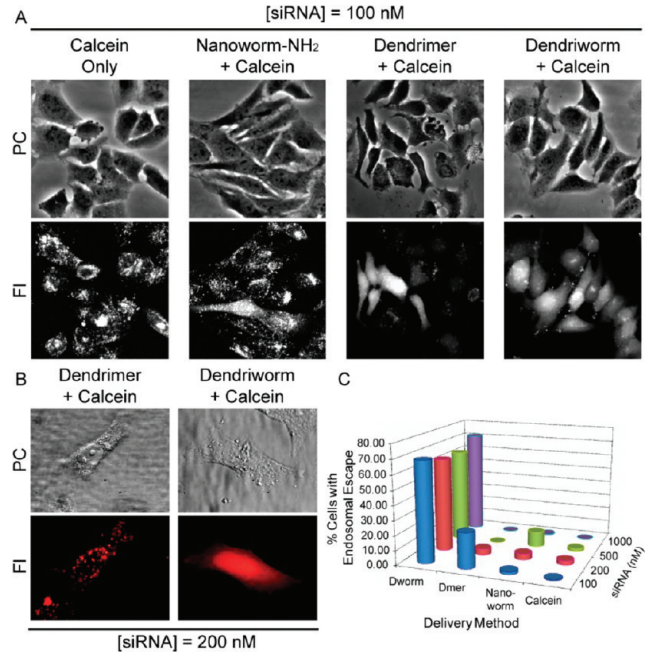

Figure 2. Dendriworms enable efficient escape of endosomal cargos. Various formulations containing varying amounts of siRNA were incubated with HeLa cells in the presence of excess Calcein for 1 h, and phase contrast (PC) and fluoresence (FL) images were taken at 20× magnification (A) or 100× magnification (B). Percent of cells with endosome escape as judged by diffuse cytoplasmic spread of Calcein was plotted to assess efficiency of siRNA delivery (C).

also dependent on uptake of the dendrimers or dendriworms into the endosomes which depends on primary amines on the surface of dendrimers that are positively charged in serum (near pH 7). Thus, addition of more negatively charged siRNAs that neutralize the positively charged primary amines may reduce the number of dendrimers or dendriworms that are able to load into the endosomes, affecting the number of buffering (tertiary) amines per endosome available for inducing endosomal escape. Indeed, when higher concentrations of siRNA were mixed with dendrimers or dendriworms, dendrimers failed to induce significant endosomal escape while dendriworms remained effective even when incubated with 1 μM siRNA (Figure 2B,C). Thus conjugation of several dendrons (reduced half of a dendrimer) onto aminated nanoworms allows for more effective endosomal escape.

Next, we examined the cytotoxicity of dendriworms at concentrations used in our studies. Two types of toxicity assays relying on either mitochondrial reductase enzyme activity (MTT assay, based on reduction of (3-(4, 5-dimethylthiazol-2-yl)-2,5-diphenyltetrazolium bromide) or on intracellular esterase activity (Calcein AM assay) were used. No significant *in vitro* toxicity across various dendriworm and siRNA concentrations used in this report was observed (Supporting Information, Figure S2).

Dendriworms Deliver siRNA into Cells and Induce Gene Silencing. We have shown that dendriworms are able to deliver cargo into cells efficiently at concentrations that have negligible toxic effects on cells *in vitro*. Next, we examined whether dendriworms could be used to deliver siRNAs into human primary glioblastoma cells (GBM-6)[47,48] that express mutant EGFRvIII, and induce gene silencing. EGFRvIII gene silencing (knockdown) in glioblastoma cells was assessed by measuring EGFR protein expression levels and the amount of mRNA transcripts compared with levels of a housekeeping gene (GAPDH) (Figure 3). Both protein and mRNA levels were suppressed significantly and were comparable to the commercial transfection agent Lipofectamine 2000 when 100 nM siRNA was delivered. Greater relative (dendriworm *vs* Lipofectamine 2000) gene silencing was observed at protein level than at mRNA level. One potential cause for this could be the dependence of mRNA read-out method (qRT-PCR) on several rounds of amplification, which may attenuate the differences if the initial number of mRNAs is different but high in two samples. Gene silencing was found to be strongly dependent on siRNA and dendriworm dose (Figure 3). The knockdown was also sequence dependent as lamin siRNA did not lower the expression levels of EGFR (Figure 3).[49] Further, EGFR siRNA delivered using aminated nanoworms or dendrimers did not produce significant EGFR knockdown (Supporting Information, Figures S4, S5). In addition to GMB-6 cells, dendriworms also produce significant gene knockdown in HeLa cells (Supporting Information, Figure S3) although, consistent with the literature on the variability of polymeric formulation dependent siRNA delivery,[50−52] the extent of knockdown in HeLa cells is lower. Taken together these results imply that dendriworms are a highly effective siRNA delivery vehicle for GBM-6 glioblastoma cells and represent a flexible for-

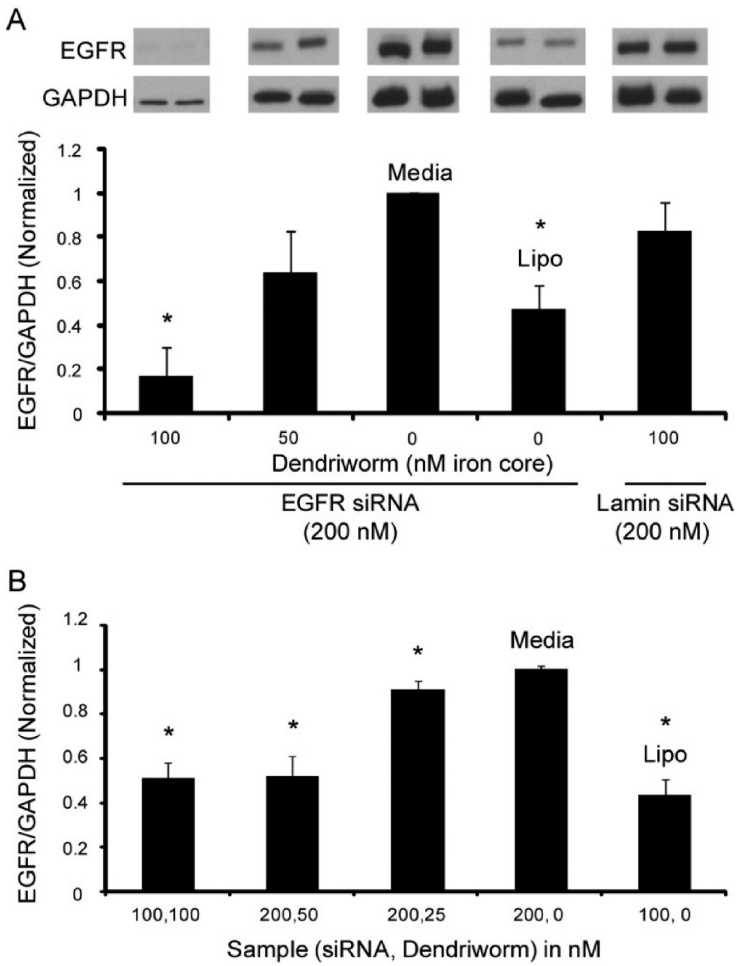

Figure 3. Delivery of EGFR siRNA into glioblastoma cells with dendriworms. (A) EGFR protein levels were assessed using Western blot with GAPDH as a housekeeping gene. Lamin siRNA was used as a control for testing sequence specificity and Lipfectamine 2000 was used as a positive control. EGFR/GAPDH expression ratio was plotted from at least three independent experiments. (B) EGFR to GAPDH mRNA transcript level ratio was calculated using qRT-PCR. Concentration of dendriworm expressed in iron core concentration. The asterisk (*) represents a *p*-value of <0.05.

mulation due to noncovalent siRNA attachment for optimization of siRNA delivery to other cell types.

Systemic Delivery of Dendriworms. We evaluated the utility of dendriworm-based siRNA delivery in mice. When dendriworms (20 μg of iron in 100 μL of 1× PBS) were injected in the bloodstream *via* tail vein injections, preferential accumulation in the lungs, as expected from the cationic nature of the particles,[53] was seen (Supporting Information, Figure S6). Briefly, Swiss Webster mice were injected in the tail vein with fluorescently labeled dendriworms and the amount of fluorescence remaining in the blood at various time points was measured. This was done by drawing blood at different time points, removing cells and debris *via* centrifugation at 800 rpm for 5 min, and measuring the fluorescence from the supernatant using an Odyssey infrared imaging system (Li-Cor Biosciences, Inc.). In this experiment, dendriworms cleared the blood within in 5 min (Supporting Information, Figure S9).

To further probe where the particles were accumulating, 100 μL of 1× PBS containing 20 μg of dendriworms or 20 μg of fluorescently labeled CLIO-NH_2 or 1× PBS alone was injected in the tail vein of mice and the mice were sacrificed after approximately 10 min of injections. After further 10 min, the organs were removed, washed with saline, and imaged with Odyssey infrared imaging system (Li-Cor Biosciences, Inc.). Since dendriworms were labeled with infrared emitting dye VivoTag680, fluorescence could be used to infer the degree of uptake of particles in various organs. Images were color coded to reflect the intensity of uptake (Supporting Information, Figure S6, left). After observing significant accumulation in the lungs (also confirmed using histology; data not shown), we sought to test if the accumulation was lung-specific. To test this, one pair of Swiss Webster mice was injected with PBS and the other pair of mice was injected with dendriworms, in the left heart ventricle. The results from this experiment are shown in the right side of Figure S6. The results show that dendriworms still accumulate in the lungs and the reticuloendothelial filtration organs.

Therefore, we sought to use dendriworms *in vivo via* means that do not depend on systemic circulation of the particles to reach the target organ or tissue (*e.g.*, intraperitoneal cavity or intravenous injections).

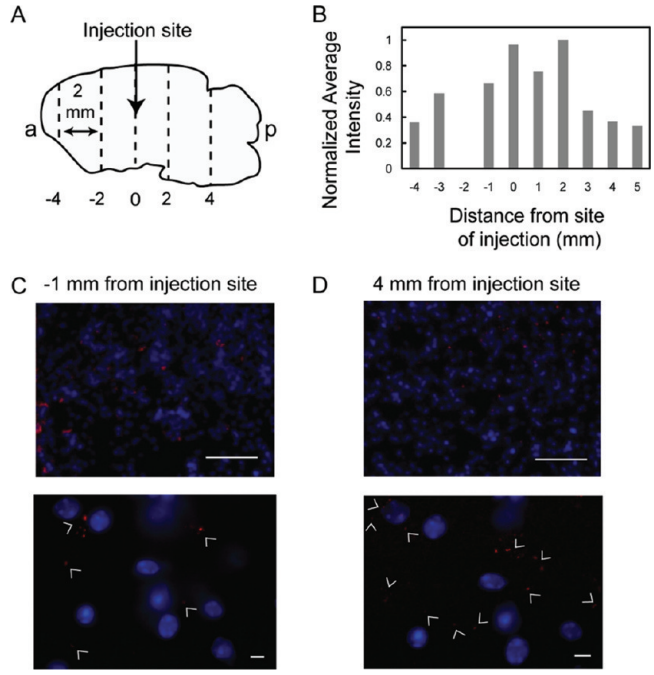

Figure 4. Biodistribution of nanoparticles in the brain. (A) Schematic representation of a sagittal mouse brain showing position of the tissue sections analyzed after 3 days of nanoparticle delivery with respect to the site of injection (a: anterior, p: posterior) (B) Quantification of nanoparticle distribution within various brain sections based on the nanoparticle fluorescence intensity (normalized to the maximum average mean intensity). (C) Images showing distribution of nanoparticles in tissue section near the site of injection (at −1 mm) and in a tissue section far from the site of injection (at 4 mm) at a lower (top image, scale bar is 100 μm) and higher (bottom image, scale bar is 500 μm) magnification. DAPI is shown in blue. The nanoparticles are color coded red and indicated by arrow heads in the higher magnification images.

Convection-Enhanced Intracranial Delivery of EGFR siRNA Using Dendriworms Reduces EGFR Expression in GBM Tumors. Given the efficacy of RNA interference in GBM cells *in vitro*, we studied the effects of siRNA delivery by dendriworms to the brain parenchyma. First, we determined the biodistribution within CNS tissues of healthy CD-1 outbred mice, by formulating 0.5 mg/mL fluorescently labeled dendriworms with 0.115 mg/mL siRNAs intracranial infusion for a period of 3 days and 7 days using an osmotic pump delivering particles at a rate of 0.5 μL/h. Particles were observed in tissue sections from both the posterior and the anterior locations with respect to the injection site for both the 3 days delivery (Figure 4) B, C, and D and 7 days delivery (Supporting Information, Figure S7). We observed that the nanoparticles were able to penetrate throughout the brain parenchyma in a distance-dependent fashion as reflected in greater fluorescence intensity levels in the tissue sections closer to the site of injection and detectable nanoparticles at the far border (Figure 4B). Dendriworms were found to be present at the perinuclear region in cells *in vivo* (Figure 4C,D and Supporting Information, Figure S7) consistent with the particles entering the cells. Histopathological evaluation of the injected animals revealed no discernible pathology at the concentration used (Supporting Information, Figure S7B), confirming the lack of carrier-induced toxicity from dendriworms. These data suggest applicability of dendriworms for siRNA delivery into CNS tissues *via* sustained, convection-enhanced delivery. On the basis of these results, a concentration of 0.5 mg/mL of dendriworm was chosen for further *in vivo* studies.

To test dendriworms' delivery efficacy *in vivo*, we used a genetically engineered mouse model of glioblastoma, in which expression of oncogenic EGFR variant III leads to *de novo* GBM tumor formation.[54] At 20 days post tumor initiation, VivoTag 680 dye-labeled dendriworms carrying an EGFR siRNA or a GFP siRNA or aminated nanoworms carrying EGFR siRNA were delivered intratumorally in brain tumor bearing animals by convection-enhanced delivery using an osmotic pump for a period of 7 days at 0.5 mg/mL of dendriworm and 0.115 mg/mL of siRNA (11 μg total siRNA). Post infusion, animals were sacrificed and immunofluorescence was performed on the tumor sections to analyze EGFR knock down. The images and the results from quantification of EGFR expression are shown in Figure 5 (also see Supporting Information, Figure S8). In the animal treated with dendriworms carrying EGFR siRNA, strong and significant suppression of EGFR expression was seen (Figure 5A,D) compared with the animal treated with dendriworms carrying GFP siRNA (Figure 5B,D) or the aminated nanoworms mixed with EGFR siRNA (Figure 5C,D). On the other hand, similar amount of nanoparticles were taken up in the brain across the three treatments (Figure 5D). In fact, even with slightly higher nanoparticle uptake in the control samples, the level of EGFR expression was much higher than in the

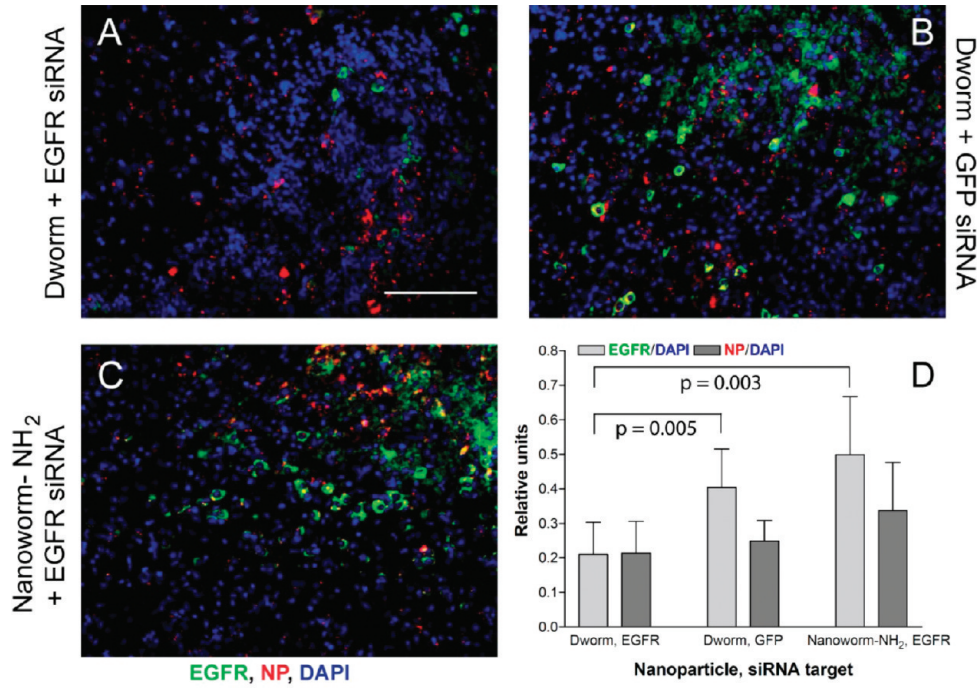

Figure 5. ***In vivo*** **knockdown of EGFR expression in transgenic mice. (A) EGFR siRNA delivered with dendriworms, (B) GFP siRNA delivered with dendriworms, (C) EGFR siRNA delivered with nanoworm-NH_2, and (D) quantitative analysis of EGFR expression per cell or nanoparticle (NP) uptake relative to number of cells (DAPI) using data from 6 separate sections from a mouse for each treatment (all images included in the Supporting Information). See Experimental Section for quantification details. Scale bar is 100 μm.**

animal treated with the dendriworm + EGFR siRNA formulation. Furthermore, distinct mismatch in location of nanoparticles and EGFR expression was seen in the sections from dendriworm + EGFR siRNA treated samples while significant overlap and even colocalization of nanoparticles with EGFR was seen in the other control samples. Using a relevant *de novo* GBM model system whereby tumor cells grow and migrate through the microenvironment similar to what is observed in human patients is necessary for ascertaining the penetrating power of dendriworms. Our data demonstrate that dendriworms are not only able to diffuse into brain tumors but can also deliver siRNA into the tumor cells, resulting in significant gene silencing *in vivo*. In this context, these results reveal that the use of dendriworms for siRNA delivery to GBM may have a clear clinical impact on this disease.

CONCLUSION

In this work, we demonstrate a systematic design-based approach to achieve siRNA delivery, both *in vitro* and *in vivo*, using dendriworms. We also demonstrate the correlation between the extent of endosomal escape and the efficiency of gene silencing. The marked enhancement in endosomal escape efficiency of dendriworms compared to dendrimers or nanoworms suggests that enrichment of polymers along the nanoworm backbone promotes improved proton sponge effect and endosomal escape, resulting in better siRNA silencing. This paradigm can be applied to other gene delivery polymers to design polyvalent, nanoparticle-based siRNA delivery agents that are effective across various cell lines and amenable to multimodal *in vivo* detection and tracking.

Using dendriworms, we also demonstrate significant suppression of EGFR expression levels in glioblastoma cells and *in vivo* in a transgenic mouse model of glioblastoma.[54] This finding has clinical significance because glioblastoma multiforme is an especially aggressive form of cancer often with elevated expression levels of EGFR.[55−58] Further, inhibition of EGFR activity has been demonstrated to be clinically beneficial in a subset of patients[59] implying that elimination of EGFR signaling through gene expression knockdown may result in positive clinical outcomes.

The combination of delivery, imaging, and targeting capabilities within dendriworms offers a versatile and powerful agent to combat malignant glioma. Availability of several primary amine groups on dendriworms makes them an attractive platform for conjugating other entities that can modulate their tumor uptake, biodistribution, and tissue homing properties. The magnetic core in dendriworms should also allow *in vivo* imaging of dendriworms *via* MR. Finally, while several methods for the delivery of nanotechnology-based therapeutics for treatment of malignant gliomas have been developed,[60] in most cases, these entities offer a single modality of detection or delivery and have proven to be toxic at functional concentrations, which is in contrast

with the low neuro-toxicity we observed with dendriworms. Thus, in conclusion, dendriworms are potent siRNA delivery nanoparticles for *in vivo* applications and offer an unprecedented versatility.

EXPERIMENTAL SECTION

Chemicals and Reagents. Unless noted otherwise, all chemical were purchased from Sigma-Aldrich, Inc. All nonproprietary siRNAs were obtained from Dharmacon, Inc.

Synthesis of Dendriworms. Cross-linked iron oxide nanoparticles were synthesized using published methods.[61,62] Briefly, 4.5 g of Dextran (*M*, 15000−25000) and 0.63 g of $FeCl_3 \cdot 6H_2O$ were dissolved in 10 mL of cold, sterile water in a round-bottom flask purged with nitrogen and kept in an ice bath. Freshly prepared solution of 0.25 g $FeCl_2 \cdot 4H_2O$ in cold 5 mL sterile water was injected into the flask while the solution was stirred at 800 rpm. Next, 1 mL of cold ammonia was added into the flask dropwise. After 10 min the reaction was allowed to proceed at 80 °C for 1 h. The resulting reaction product was diluted 1:4 in sterile water and filtered (Amicon Ultra-4 MWCO: 100 000). Finally, the particles were filtered using 0.2 μm, 32 mm syringe filters (Pall Corporation, East Hills, NY) to remove large particles and aggregates. A 1.5 mL alilquot of particles was cross-linked by adding a mixture of 2.5 mL of 5 M NaOH and 1 mL of epicholohydrin and allowing the reaction to proceed with stirring at room temperature for 24 h. Resulting particles were dialyzed using 50 000 MWCO membrane and aminated overnight by adding 10% ammonia.

Cross-linked, aminated iron oxide particles were activated with 500-fold excess of SPDP (*N*-succinimidyl 3-(2-pyridyldithio)-propionate, Pierce Biotechnology, Inc.) and reacted with VivoTag680 (Visen Medical, Inc.). The particles were filtered using a G50 (GE Healthcare) sephadex column. Next, Cystamine core, PAMAM dendrimers were reduced using 0.5 M DTT (dithiothreitol) by reacting at room temperature for 2 h. Excess DTT was removed using G25 column and reduced PAMAM dendrons were mixed with the SPDP-activated magnetic particles and allowed to react overnight at room temperature with gentle shaking. Resulting particles were separated from free dendrons by filtering several times using 100 000 molecular weight cutoff filter (Amicon Ultra, Millipore, Corp.), magnetic separation column (MACS, Miltenyi Biotech) and G50 chromatography columns.

Particle Characterization. Concentration of nanoparticles was measured as iron core concentration by measuring absorbance at 400 nm. VivoTag concentration was measured using absorbance at 670 nm, and Dendron concentration was estimated by using ninhydrin reagent and fluorescamine assays. Naoparticle charge and size was measured using zeta-potential and dynamic light scattering instrument (Zetasizer-Nano, Malvern, Inc.). siRNA-nanoparticle binding was characterized *via* electrophoresis of the nanoparticle-siRNA (10 min incubation at room temperature) mixture on a 15% TBE gel (BioRad Laboratories) and staining siRNAs with SYBR Gold (Invitrogen, Inc.). The gel was visualized using UV illumination and a SYBR green filter. For studying the stability of the siRNA−dendriworm nanoparticle, we complexed the siRNA with the dendriworms for 10 min and added ACSF to the nanoparticle solution. ACSF was prepared by making an aqueous solution of 30 mM NaCl, 0.3 mM $CaCl_2$, 0.5 mM $MgCl_2$, 0.3 mM Na_2HPO_4, 5.2 mM $NaHCO_3$, and the pH was adjusted to 7.44. The siRNA−dendriworm nanoparticles were incubated in ACSF at 37 °C for the specified times and 1% SDS was added to release the bound siRNA. The samples were analyzed for residual siRNA by electrophoresis on a 15% TBE gel using a similar procedure as described above.

Endosome Escape Assay. Membrane impermeable dye Calcein (0.25 mM) or FITC-conjugated dextran (10 000 MW) were codelivered with the various nanoparticle formulations. After 1 h, excess dye was washed off, and cells were visualized with a fluorescence imaging system. Ratio of number of cells with endosome escape (indicated by a diffuse cytoplasmic fluorescence) and total number of cells counted from the phase contrast image was plotted to quantify the results.

Toxicity Assessment. MTT and Calcein AM assays were performed using HeLa cells in 96-well plates. Nanoparticle formulations at various concentrations were incubated with the cells for 4 or 24 h. Cells were then washed three times and the reagents were added. For MTT assay, the absorbance was read at 570 nm after 4 h. For Calcein AM assay, cells were incubated with Calcein AM for 30 min and a fluorimeter was used with 485 nm excitation and fluorescence was read at 530 nm. Data were analyzed using Graph Pad Prism 3.03.

Convection Mediated Delivery of Nanoformulations. All of the mice used in this study were maintained and handled under protocols approved by the Committee on Animal Care at the Massachusetts Institute of Technology and IACUC at Tufts University. Osmotic minipumps (Alzet mini-osmotic pump, model 2007, Durect Corp., Cupertino, CA) that maintain a constant flow over 3 or 7 days at 0.5 μL/h were implanted 20 days post tumor induction. The pump reservoir was filled with the dendriworms at 0.5 mg/mL. The reservoirs were connected to an intracranial cannula (Plastics One, Roanoke, VA) through a catheter (Durect Corp., Cupertino, CA) and implanted subcutaneously posterior to the site of tumor cell implantation, until it rested on the back of the mice. After 3 days or 7 days, the animals were sacrificed and brains were processed as described above.

Histological Analysis of Tumors, Immunofluorescence, and Antibodies. The brains were excised and prepared for histopathological analysis as follows: animals were deeply anesthetized with Nembutol and transcardially perfused with PBS followed by freshly made 4% paraformaldehyde in 0.1 M phosphate buffer, pH 7.4. The brains were excised and postfixed in the same fixative at 4 °C for 1 h, rinsed in PBS, and serial coronal sections were cut using a brain mold. Tissues embedded in paraffin and sectioned were stained with hematoxylin and eosin. For immunofluorescence, brains were excised and prepared for cryostat-frozen sectioning. Sections 10−12 um thick were then processed for indirect immunofluorescence against the EGF receptor using a rabbit polyclonal antibody (anti EGFR #2232, Cell Signaling Technology) followed by a FITC-conjugated secondary goat antirabbit antibody.

Image Processing for Quantification of EGFR Expression and Nanoparticle Uptake. Images of histological sections were acquired using either a 100× magnification oil objective or a 20× magnification objective on an inverted epifluorescence microscope (Nikon Instruments, Melville, NY) fitted with a mercury arc lamp. Standard FITC and DAPI filter cubes were used for FITC-antibody and DAPI nuclear stains. For VivoTag680 labeled nanoparticles, Texas Red filter cube was used. Images were collected using Coolsnap ES camera (Roper Scientific Instruments, Acton, MA) and Metamorph software at 2 × 2 binning with fixed exposure time for each color, across all samples. Background for each image was determined using intensity histogram and subtracted using Image J (National Institutes of Health). Images were then pseudocolored and combined to produce composites that are shown in Figures 4, and 5 and in the supplementary figures. Number of green, red, or blue pixels in each image set was used to quantify EGFR expression or nanoparticle uptake with respect to number of cells (blue pixels). Data from at least five RGB image sets were pooled to produce graph, standard deviation, and *p*-values. Since we are looking at reduction in EGFR expression, one tailed *p*-values were calculated. This was done by using using TTEST(array1, array2, 1,3) function in Microsoft Excel which does not assume distributions with equal variance. Data were plotted using Graph Pad Prizm software.

Gene Knockdown Assessment (Flow Cytometry, Western Blot, and qRT-PCR). For gene silencing experiments, siRNA delivery formulations were incubated with the cells for 4 h in serum free medium. Then, 10% serum containing medium was used to replace the serum-free medium. Lipofectamine 2000 was used as per supplier protocols (Invitrogen, Inc.), at concentrations shown in the figures (*e.g.*, 100 or 200 nM). All experiments were performed in 96-well plates with ~6000 cells at the time of starting experiment in 150 μL of final volume including cell culture medium and other reagents. For GFP knockdown assessment, (GFP siRNA

sense strand: 5′-GG CUA CGU CCA GGA GCG CAC C-3′) cells were left in the cell culture incubator for 48 h; for EGFR knockdown assessment, cells were incubated for 72 h. After the incubation period, cells were trypsinized and resuspended in cold 1× PBS containing 1% fetal bovine serum. Reduction in GFP expression was measured using flow cytometry; EGFR protein and mRNA levels were measured using Western blot and quantitative RT-PCR (Bio-Rad iCycler). Primary antibodies for Western blots were purchased from Cell Signaling (EGF receptor antibody: catalog no. 2232 and GAPDH antibody: catalog no. 2118). Western blots were developed using HRP-secondary antibody along with the SuperSignal West Pico substrate (Pierce Biotechnology, Inc.). Primers for EGFR and GAPDH mRNA amplification and quantification *via* qRT-PCR were obtained from Integrated DNA Technologies: (EGFR forward primer) TAGAAATCATACGCGGCAGGACCA, (reverse primer) TCAGGCTGACGACTGCAAGAGAAA; (GAPDH forward primer) TCGACAGTCAGCCGCATCTTCTT, (reverse primer) ACCAAATCCGTTGACTCCGACCTT.

Acknowledgment. We thank Greg Underhill for help with Q-RT-PCR, Sandra March for help with the western blots, Margarita Akiyama with toxicity analysis, Erika Batchelder of the Keck imaging facility at the Whitehead Institute at MIT for help with transmission electron micrographs, and Muthiah Manoharan and colleagues at Alnylam for helpful discussions. A.A. acknowledges support from David H. Koch Cancer Research Fund and from the MIT-Harvard CCNE fellowship. This work was supported by NIH BRP CA124427and NIH CA119349. This work is supported in part by the Cam Neely Foundation (A.C. and H.Z.). P.A.S. acknowledges the generous support from the Pierre Casimir-Lambert Fund.

Supporting Information Available: Figures S1−S9. This material is available free of charge *via* the Internet at http://pubs.acs.org.

REFERENCES AND NOTES

1. Fire, A.; Xu, S.; Montgomery, M. K.; Kostas, S. A.; Driver, S. E.; Mello, C. C. Potent and Specific Genetic Interference by Double-Stranded RNA in Caenorhabditis Elegans. *Nature* **1998**, *391*, 806–11.
2. Devi, G. R. siRNA-Based Approaches in Cancer Therapy. *Cancer Gene Ther.* **2006**, *13*, 819–29.
3. Takeshita, F.; Ochiya, T. Therapeutic Potential of RNA Interference against Cancer. *Cancer Sci.* **2006**, *97*, 689–96.
4. Elbashir, S. M.; Harborth, J.; Lendeckel, W.; Yalcin, A.; Weber, K.; Tuschl, T. Duplexes of 21-Nucleotide RNAs Mediate RNA Interference in Cultured Mammalian Cells. *Nature* **2001**, *411*, 494–8.
5. Dorsett, Y.; Tuschl, T. Sirnas: Applications in Functional Genomics and Potential as Therapeutics. *Nat. Rev. Drug Discovery* **2004**, *3*, 318–29.
6. Stevenson, M. Therapeutic Potential of RNA Interference. *New. Engl. J. Med.* **2004**, *351*, 1772–7.
7. Dykxhoorn, D. M.; Palliser, D.; Lieberman, J. The Silent Treatment: siRNAs as Small Molecule Drugs. *Gene Ther.* **2006**, *13*, 541–52.
8. Uprichard, S. L. The Therapeutic Potential of RNA Interference. *FEBS Lett.* **2005**, *579*, 5996–6007.
9. Novina, C. D.; Murray, M. F.; Dykxhoorn, D. M.; Beresford, P. J.; Riess, J.; Lee, S. K.; Collman, R. G.; Lieberman, J.; Shankar, P.; Sharp, P. A. siRNA-Directed Inhibition of HIV-1 Infection. *Nat. Med.* **2002**, *8*, 681–6.
10. Soutschek, J.; Akinc, A.; Bramlage, B.; Charisse, K.; Constien, R.; Donoghue, M.; Elbashir, S.; Geick, A.; Hadwiger, P.; Harborth, J.; *et al*. Therapeutic Silencing of an Endogenous Gene by Systemic Administration of Modified siRNAs. *Nature* **2004**, *432*, 173–8.
11. Zimmermann, T. S.; Lee, A. C. H.; Akinc, A.; Bramlage, B.; Bumcrot, D.; Fedoruk, M. N.; Harborth, J.; Heyes, J. A.; Jeffs, L. B.; John, M.; *et al*. RNAi-Mediated Gene Silencing in Non-Human Primates. *Nature* **2006**, *441*, 111–14.
12. Song, E.; Zhu, P.; Lee, S. K.; Chowdhury, D.; Kussman, S.; Dykxhoorn, D. M.; Feng, Y.; Palliser, D.; Weiner, D. B.; Shankar, P.; *et al*. Antibody Mediated *in Vivo* Delivery of Small Interfering RNAs *via* Cell-Surface Receptors. *Nat. Biotechnol.* **2005**, *23*, 709–17.
13. Akinc, A.; Zumbuehl, A.; Goldberg, M.; Leshchiner, E. S.; Busini, V.; Hossain, N.; Bacallado, S. A.; Nguyen, D. N.; Fuller, J.; Alvarez, R.; *et al*. A Combinatorial Library of Lipid-Like Materials for Delivery of RNAi Therapeutics. *Nat. Biotechnol.* **2008**, *26*, 561–9.
14. Li, S. D.; Chono, S.; Huang, L. Efficient Oncogene Silencing and Metastasis Inhibition *via* Systemic Delivery of siRNA. *Mol. Ther.* **2008**, *16*, 942–6.
15. Landen, C. N.; Merritt, W. M.; Mangala, L. S.; Sanguino, A. M.; Bucana, C.; Lu, C.; Lin, Y. G.; Han, L. Y.; Kamat, A. A.; Schmandt, R.; *et al*. Intraperitoneal Delivery of Liposomal siRNA for Therapy of Advanced Ovarian Cancer. *Cancer Biol. Ther.* **2006**, *5*, 1708–13.
16. Yezhelyev, M. V.; Qi, L.; O'Regan, R. M.; Nie, S.; Gao, X. Proton-Sponge-Coated Quantum Dots for siRNA Delivery and Intracellular Imaging. *J. Am. Chem. Soc.* **2008**, *130*, 9006–12.
17. Medarova, Z.; Pham, W.; Farrar, C.; Petkova, V.; Moore, A. *In Vivo* Imaging of siRNA Delivery and Silencing in Tumors. *Nat. Med.* **2007**, *13*, 372–7.
18. Oishi, M.; Nakaogami, J.; Ishii, T.; Nagasaki, Y. Smart Pegylated Gold Nanoparticles for the Cytoplasmic Delivery of siRNA to Induce Enhanced Gene Silencing. *Chem. Lett.* **2006**, *35*, 1046–7.
19. Rosi, N. L.; Giljohann, D. A.; Thaxton, C. S.; Lytton-Jean, A. K.; Han, M. S.; Mirkin, C. A. Oligonucleotide-Modified Gold Nanoparticles for Intracellular Gene Regulation. *Science* **2006**, *312*, 1027–30.
20. Liu, Z.; Winters, M.; Holodniy, M.; Dai, H. siRNA Delivery into Human T Cells and Primary Cells with Carbon-Nanotube Transporters. *Angew. Chem., Int. Ed.* **2007**, *46*, 2023–7.
21. KukowskaLatallo, J. F.; Bielinska, A. U.; Johnson, J.; Spindler, R.; Tomalia, D. A.; Baker, J. R. Efficient Transfer of Genetic Material into Mammalian Cells Using Starburst Polyamidoamine Dendrimers. *Proc. Natl. Acad. Sci. U.S.A.* **1996**, *93*, 4897–4902.
22. Tomalia, D. A.; Baker, H.; Dewald, J.; Hall, M.; Kallos, G.; Martin, S.; Roeck, J.; Ryder, J.; Smith, P. A New Class of Polymers—Starburst-Dendritic Macromolecules. *Polym. J.* **1985**, *17*, 117–32.
23. Tomalia, D. A.; Frechet, J. M. J. Discovery of Dendrimers and Dendritic Polymers: A Brief Historical Perspective. *J. Polym. Sci., Part A* **2002**, *40*, 2719–28.
24. Shi, X. Y.; Thomas, T. P.; Myc, L. A.; Kotlyar, A.; Baker, J. R. Synthesis, Characterization, and Intracellular Uptake of Carboxyl-Terminated Poly(Amidoamine) Dendrimer-Stabilized Iron Oxide Nanoparticles. *Phys. Chem. Chem. Phys.* **2007**, *9*, 5712–20.
25. Luo, D.; Haverstick, K.; Belcheva, N.; Han, E.; Saltzman, W. M. Poly(ethylene glycol)-Conjugated PAMAM Dendrimer for Biocompatible, High-Efficiency DNA Delivery. *Macromolecules* **2002**, *35*, 3456–62.
26. Kono, K.; Akiyama, H.; Takahashi, T.; Takagishi, T.; Harada, A. Transfection Activity of Polyamidoamine Dendrimers Having Hydrophobic Amino Acid Residues in the Periphery. *Bioconjug. Chem.* **2005**, *16*, 208–14.
27. Myc, A.; Patri, A. K.; Baker, J. R. Dendrimer-Based BH3 Conjugate That Targets Human Carcinoma Cells. *Biomacromolecules* **2007**, *8*, 2986–9.
28. Shukla, R.; Thomas, T. P.; Peters, J.; Kotlyar, A.; Myc, A.; Baker, J. R. Tumor Angiogenic Vasculature Targeting with PAMAM Dendrimer-RGD Conjugates. *Chem Commun.* **2005**, 5739–41.
29. Bi, X.; Shi, X.; Majoros, I. J.; Shukla, R.; Baker, J. R. Multifunctional Poly(amidoamine) Dendrimer-Taxol Conjugates: Synthesis, Characterization and Stability. *J. Comput. Theor. Nanosci.* **2007**, *4*, 1179–87.
30. Lee, C. C.; Gillies, E. R.; Fox, M. E.; Guillaudeu, S. J.; Frechet, J. M. J.; Dy, E. E.; Szoka, F. C. A Single Dose of Doxorubicin-Functionalized Bow-Tie Dendrimer Cures Mice Bearing C-26 Colon Carcinomas. *Proc. Natl. Acad. Sci. U.S.A.* **2006**, *103*, 16649–54.

31. Najlah, M.; Freeman, S.; Attwood, D.; D'Emanuele, A. Synthesis and Assessment of First-Generation Polyamidoamine Dendrimer Prodrugs to Enhance the Cellular Permeability of P-Gp Substrates. *Bioconjug. Chem.* **2007**, *18*, 937–46.
32. Choi, Y.; Baker, J. R. Targeting Cancer Cells with DNA-Assembled Dendrimers—A Mix and Match Strategy for Cancer. *Cell Cycle* **2005**, *4*, 669–71.
33. Landmark, K. J.; DiMaggio, S.; Ward, J.; Kelly, C.; Vogt, S.; Hong, S.; Kotlyar, A.; Myc, A.; Thomas, T. P.; Penner-Hahn, J. E.; *et al*. Synthesis, Characterization, and *in Vitro* Testing of Superparamagnetic Iron Oxide Nanoparticles Targeted Using Folic Acid-Conjugated Dendrimers. *ACS Nano* **2008**, *2*, 773–83.
34. Kobayashi, H.; Jo, S. K.; Kawamoto, S.; Yasuda, H.; Hu, X.; Knopp, M. V.; Brechbiel, M. W.; Choyke, P. L.; Star, R. A. Polyamine Dendrimer-Based MRI Contrast Agents for Functional Kidney Imaging to Diagnose Acute Renal Failure. *J. Magn. Reson. Imag.* **2004**, *20*, 512–8.
35. Lee, C. C.; MacKay, J. A.; Frechet, J. M.; Szoka, F. C. Designing Dendrimers for Biological Applications. *Nat. Biotechnol.* **2005**, *23*, 1517–26.
36. Dufes, C.; Uchegbu, I. F.; Schatzlein, A. G. Dendrimers in Gene Delivery. *Adv. Drug Delivery Rev.* **2005**, *57*, 2177–202.
37. Kang, H.; DeLong, R.; Fisher, M. H.; Juliano, R. L. Tat-Conjugated PAMAM Dendrimers as Delivery Agents for Antisense and siRNA Oligonucleotides. *Pharm. Res.* **2005**, *22*, 2099–106.
38. Juliano, R. L. Intracellular Delivery of Oligonucleotide Conjugates and Dendrimer Complexes. *Ann. N.Y. Acad. Sci.* **2006**, *1082*, 18–26.
39. Inoue, Y.; Kurihara, R.; Tsuchida, A.; Hasegawa, M.; Nagashima, T.; Mori, T.; Niidome, T.; Katayama, Y.; Okitsu, O. Efficient Delivery of siRNA Using Dendritic Poly(L-lysine) for Loss-of-Function Analysis. *J. Controlled Release* **2008**, *126*, 59–66.
40. Zhou, J.; Wu, J.; Hafdi, N.; Behr, J. P.; Erbacher, P.; Peng, L. PAMAM Dendrimers for Efficient siRNA Delivery and Potent Gene Silencing. *Chem Commun.* **2006**, 2362–4.
41. Shen, X. C.; Zhou, J.; Liu, X.; Wu, J.; Qu, F.; Zhang, Z. L.; Pang, D. W.; Quelever, G.; Zhang, C. C.; Peng, L. Importance of Size-to-Charge Ratio in Construction of Stable and Uniform Nanoscale RNA/Dendrimer Complexes. *Org. Biomol. Chem.* **2007**, *5*, 3674–81.
42. Duncan, R.; Izzo, L. Dendrimer Biocompatibility and Toxicity. *Adv. Drug Delivery Rev.* **2005**, *57*, 2215–37.
43. Park, J. H.; von Maltzahn, G.; Zhang, L. L.; Schwartz, M. P.; Ruoslahti, E.; Bhatia, S. N.; Sailor, M. J. Magnetic Iron Oxide Nanoworms for Tumor Targeting and Imaging. *Adv. Mater.* **2008**, *20*, 1630–5.
44. Cho, Y. W.; Kim, J. D.; Park, K. Polycation Gene Delivery Systems: Escape from Endosomes to Cytosol. *J. Pharm. Pharmacol.* **2003**, *55*, 721–34.
45. Hu, Y.; Litwin, T.; Nagaraja, A. R.; Kwong, B.; Katz, J.; Watson, N.; Irvine, D. J. Cytosolic Delivery of Membrane-Impermeable Molecules in Dendritic Cells Using pH-Responsive Core-Shell Nanoparticles. *Nano Lett.* **2007**, *7*, 3056–64.
46. Jones, R. A.; Cheung, C. Y.; Black, F. E.; Zia, J. K.; Stayton, P. S.; Hoffman, A. S.; Wilson, M. R. Poly(2-alkylacrylic acid) Polymers Deliver Molecules to the Cytosol by pH-Sensitive Disruption of Endosomal Vesicles. *Biochem. J.* **2003**, *372*, 65–75.
47. Giannini, C.; Sarkaria, J. N.; Saito, A.; Uhm, J. H.; Galanis, E.; Carlson, B. L.; Schroeder, M. A.; James, C. D. Patient Tumor EGFR and PDGFRA Gene Amplifications Retained in an Invasive Intracranial Xenograft Model of Glioblastoma Multiforme. *Neuro. Oncol.* **2005**, *7*, 164–76.
48. Sarkaria, J. N.; Carlson, B. L.; Schroeder, M. A.; Grogan, P.; Brown, P. D.; Giannini, C.; Ballman, K. V.; Kitange, G. J.; Guha, A.; Pandita, A.; *et al*. Use of an Orthotopic Xenograft Model for Assessing the Effect of Epidermal Growth Factor Receptor Amplification on Glioblastoma Radiation Response. *Clin. Cancer Res.* **2006**, *12*, 2264–71.
49. Derfus, A. M.; Chen, A. A.; Min, D. H.; Ruoslahti, E.; Bhatia, S. N. Targeted Quantum Dot Conjugates for siRNA Delivery. *Bioconjug. Chem.* **2007**, *18*, 1391–6.
50. von Gersdorff, K.; Sanders, N. N.; Vandenbroucke, R.; De Smedt, S. C.; Wagner, E.; Ogris, M. The Internalization Route Resulting in Successful Gene Expression Depends on Both Cell Line and Polyethylenimine Polyplex Type. *Mol. Ther.* **2006**, *14*, 745–53.
51. Schaffert, D.; Wagner, E. Gene Therapy Progress and Prospects: Synthetic Polymer-Based Systems. *Gene Ther.* **2008**, *15*, 1131−38.
52. Lai, S. K.; Hida, K.; Chen, C.; Hanes, J. Characterization of the Intracellular Dynamics of a Non-degradative Pathway Accessed by Polymer Nanoparticles. *J. Controlled Release* **2008**, *125*, 107–11.
53. Uyechi, L. S.; Gagne, L.; Thurston, G.; Szoka, F. C., Jr. Mechanism of Lipoplex Gene Delivery in Mouse Lung: Binding and Internalization of Fluorescent Lipid and DNA Components. *Gene Ther.* **2001**, *8*, 828–36.
54. Zhu, H.; Acquaviva, J.; Ramachandran, P.; Boskovitz, A.; Woolfenden, S.; Pfannl, R.; Bronson, R. T.; Chen, J. W.; Weissleder, R.; Housman, D. E.; *et al*. Oncogenic EGFR Signaling Cooperates with Loss of Tumor Suppressor Gene Functions in Gliomagenesis. *Proc. Natl. Acad. Sci. U.S.A.* **2009**, *106*, 2712−6.
55. Nicholas, M. K.; Lukas, R. V.; Jafri, N. F.; Faoro, L.; Salgia, R. Epidermal Growth Factor Receptor—Mediated Signal Transduction in the Development and Therapy of Gliomas. *Clin. Cancer Res.* **2006**, *12*, 7261–70.
56. Belda-Iniesta, C.; de Castro Carpeno, J.; Sereno, M.; Gonzalez-Baron, M.; Perona, R. Epidermal Growth Factor Receptor and Glioblastoma Multiforme: Molecular Basis for a New Approach. *Clin. Transl. Oncol.* **2008**, *10*, 73–7.
57. Friedman, H. S.; Bigner, D. D. Glioblastoma Multiforme and the Epidermal Growth Factor Receptor. *N Engl J Med.* **2005**, *353*, 1997–9.
58. Halatsch, M. E.; Schmidt, U.; Behnke-Mursch, J.; Unterberg, A.; Wirtz, C. R. Epidermal Growth Factor Receptor Inhibition for the Treatment of Glioblastoma Multiforme and Other Malignant Brain Tumours. *Cancer Treat Rev.* **2006**, *32*, 74–89.
59. Mellinghoff, I. K.; Wang, M. Y.; Vivanco, I.; Haas-Kogan, D. A.; Zhu, S.; Dia, E. Q.; Lu, K. V.; Yoshimoto, K.; Huang, J. H.; Chute, D. J.; *et al*. Molecular Determinants of the Response of Glioblastomas to EGFR Kinase Inhibitors. *New Engl. J. Med.* **2005**, *353*, 2012–24.
60. Jain, K. K. Nanobiotechnology-Based Drug Delivery to the Central Nervous System. *Neurodegener. Dis.* **2007**, *4*, 287–91.
61. Josephson, L.; Tung, C. H.; Moore, A.; Weissleder, R. High-Efficiency Intracellular Magnetic Labeling with Novel Superparamagnetic-Tat Peptide Conjugates. *Bioconjug. Chem.* **1999**, *10*, 186–91.
62. Palmacci, S.; Josephson, L. Synthesis of Polysaccharide Covered Superparamagnetic Oxide Colloids. U.S. Patent 5,262,176, 1993.

Functional Delivery of siRNA in Mice using Dendriworms

Supporting Information

*Amit Agrawal, Dal-Hee Min, Neetu Singh, Haihao Zhu, Alona Birjiniuk, Geoffrey von Maltzahn, Todd J Harris, Deyin Xing, Stephen D. Woolfenden , Phillip A. Sharp, Alain Charest and Sangeeta Bhatia**

* To whom correspondence should be addressed:

Prof. Sangeeta N. Bhatia

77 Massachusetts Ave., Bldg. E19-502d

Cambridge, MA 02139, USA

E-mail: sbhatia@mit.edu

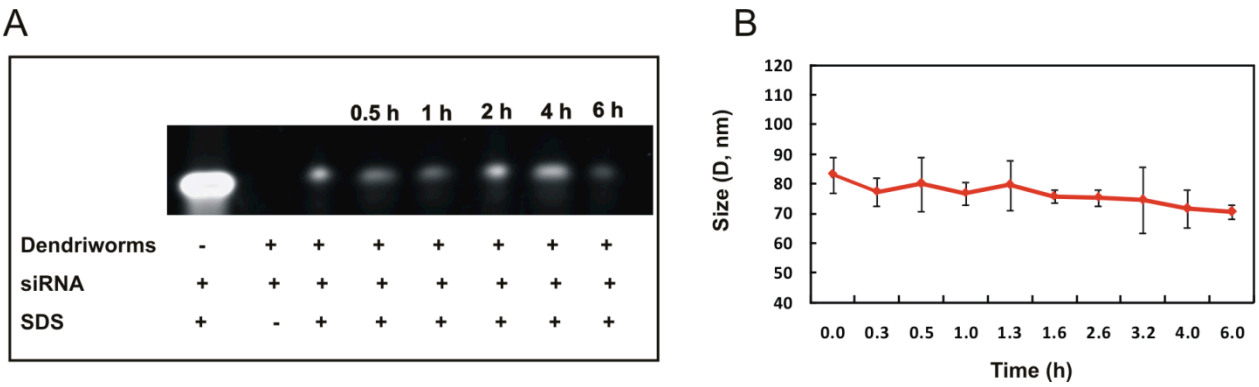

Figure S1: Stability of siRNA-Dendriworm nanoparticle in artificial cerebrospinal fluid (ACSF). (A) Gel electrophoresis indicating the stability of siRNA in ACSF. (B) DLS of the siRNA-Dendriworm complex in ACSF indicating colloidal stablility over time.

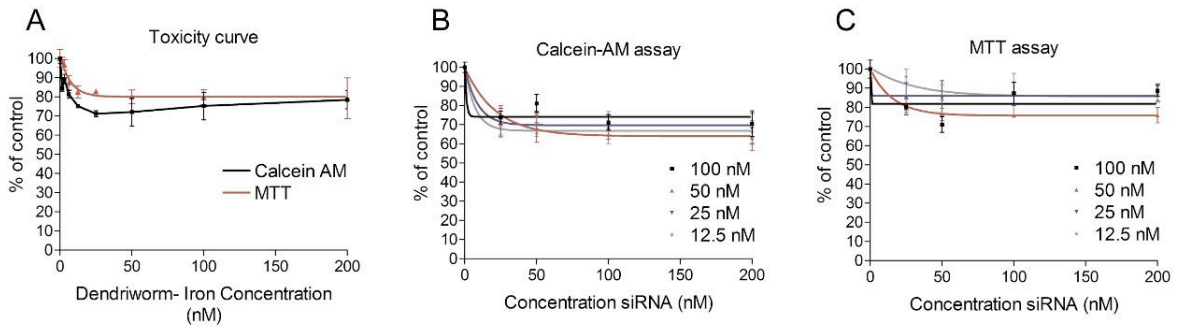

Figure S2. (A) Calcein AM and MTT toxicity assays with Dendriworms incubated with HeLa cells. Formulations were incubated using a protocol similar to that used for assessment of siRNA mediated gene silencing (4 hour incubation with nanoparticle containing solution followed by 20 hours of incubation in cell culture medium) and viability was assessed 24 hours later (B) Calcein AM toxicity assay with varying Dendriworm and siRNA concentrations following the same protocol as in A (C) MTT toxicity assay with varying Dendriworm and siRNA concentrations following the same protocol as in A. Toxicity was also assessed immediately after 4 hour incubation with the nanoparticle formulations (data not shown) and no formulation was found to reduce the viability below 50%.

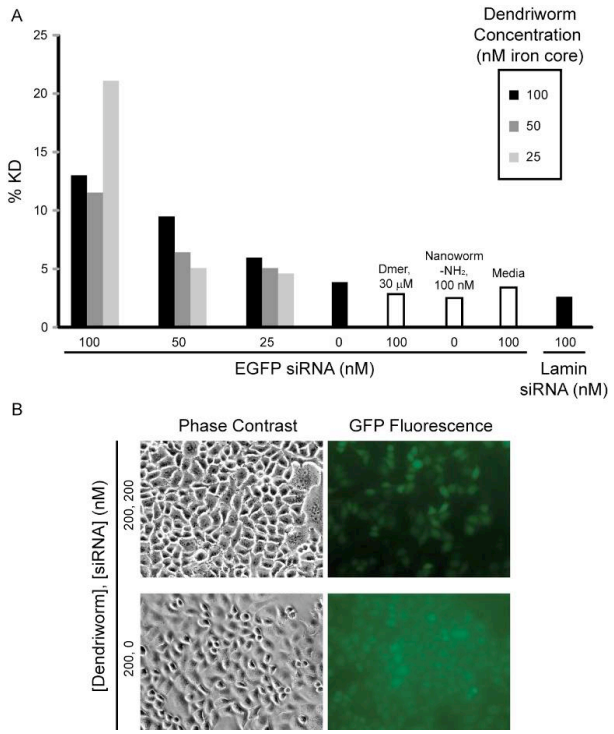

Figure S3. GFP knockdown in HeLa cells. HeLa-GFP cells were incubated with dendriworms at different siRNA and dendriworm concentrations (nM iron) and dose dependent GFP knockdown was observed. The knockdown was low but significant when compared with various controls (dendrimer only, nanoworm-NH2, Lamin siRNA treatment or no treatment). Lipofectamine 2000 produced as high as 70-80% knockdown in these experiments when 100 or 50 nM siRNA was used. Nanoworm concentration expressed as iron core concentration.

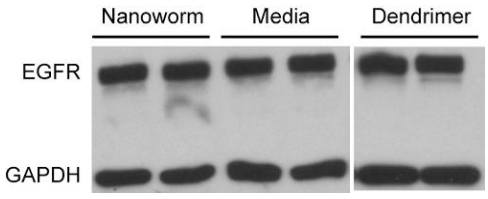

Figure S4. Controls for EGFR siRNA delivery in GBM-6 cells with dendriworms. No difference in EGFR/GAPDH ratio was seen for any of MION, dendrimer treatment or no treatment conditions.

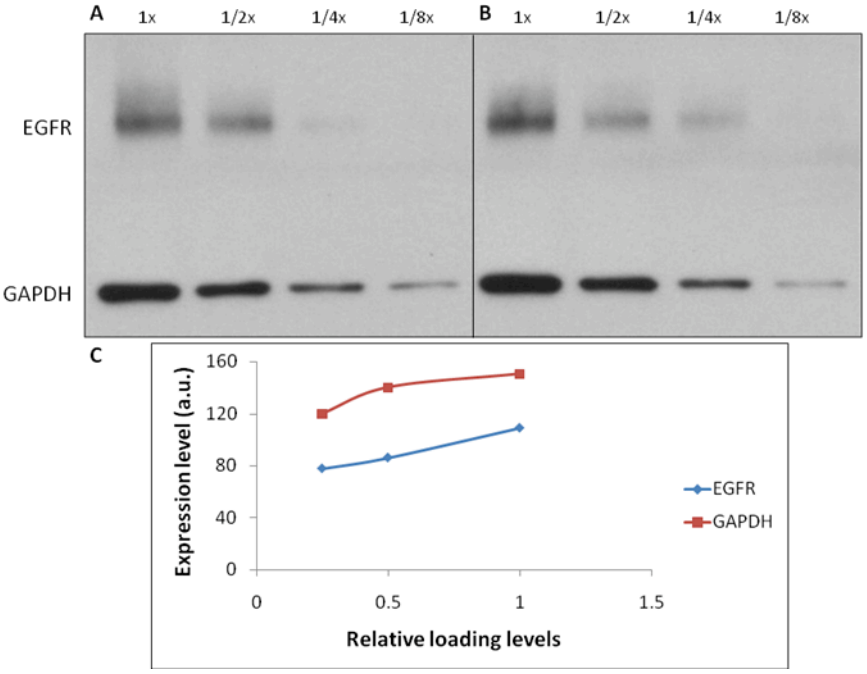

Figure S5. EGFR/GAPDH ratio is linear over the range of band intensities analyzed in the manuscript. A,B: Series dilutions of protein lysate obtained from GBM-6 cells were tested for EGFR and GAPDH protein levels via western blot. C: Quantification of band intensities in A and B reveals linear and proportional increas in EGFR and GAPDH levels as concentration increases.

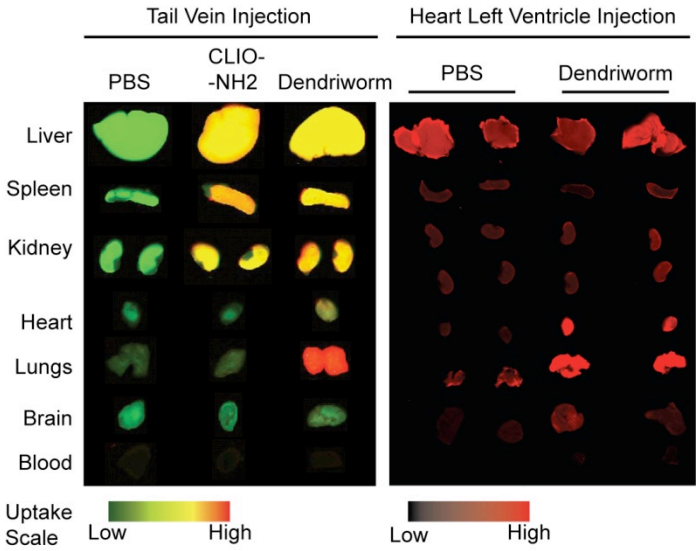

Figure S6. Biodistribution of dendriworms *in vivo* when injected sytemically. (Left): When dendriworms are injected in the tail vein of a Swiss Webster mouse, they accumulate in the lungs within 5 minutes while CLIO-NH_2 particles do not exhibit this behavior and end up in the liver, spleen and

kidneys (Right): dendriworms home to the lungs even when injected into the heart left ventricle of Swiss Webster mouse so that they arrive at the lungs the last. Heart left ventricle injections were done in duplicate, at the same time to eliminate potential error arising from accidental right ventricle injection. The gradient scales indicate least uptake on the left end and the maximum uptake at the right end.

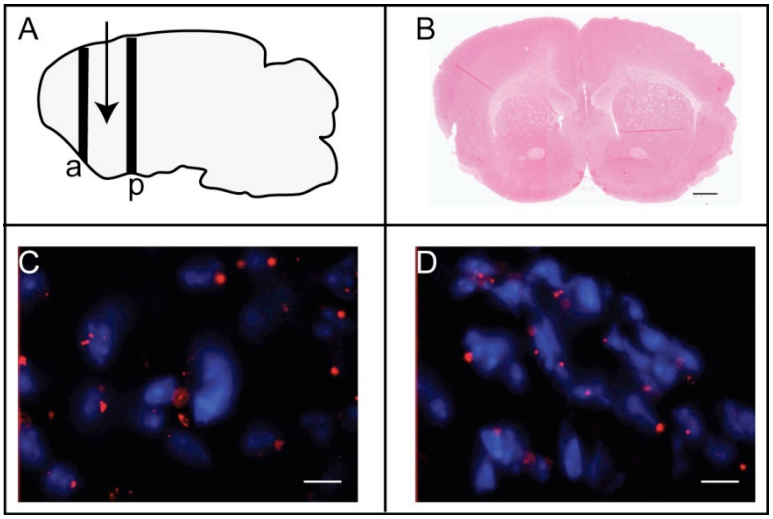

Figure S7. Dendriworms formulated with siRNA are well tolerated in the brain tissue. A) Sagittal schematic representation of a mouse brain indicating the site of injection (arrow). B) Coronal H&E stained paraffin-embedded section at the site of injection. Scale bar is 500 μm. The nanoparticles penetrate in both the anterior (a, C) and posterior (p, D) directions from the site of injection after 7 days of delivery. Scale bars in C and D are 10 μm long.

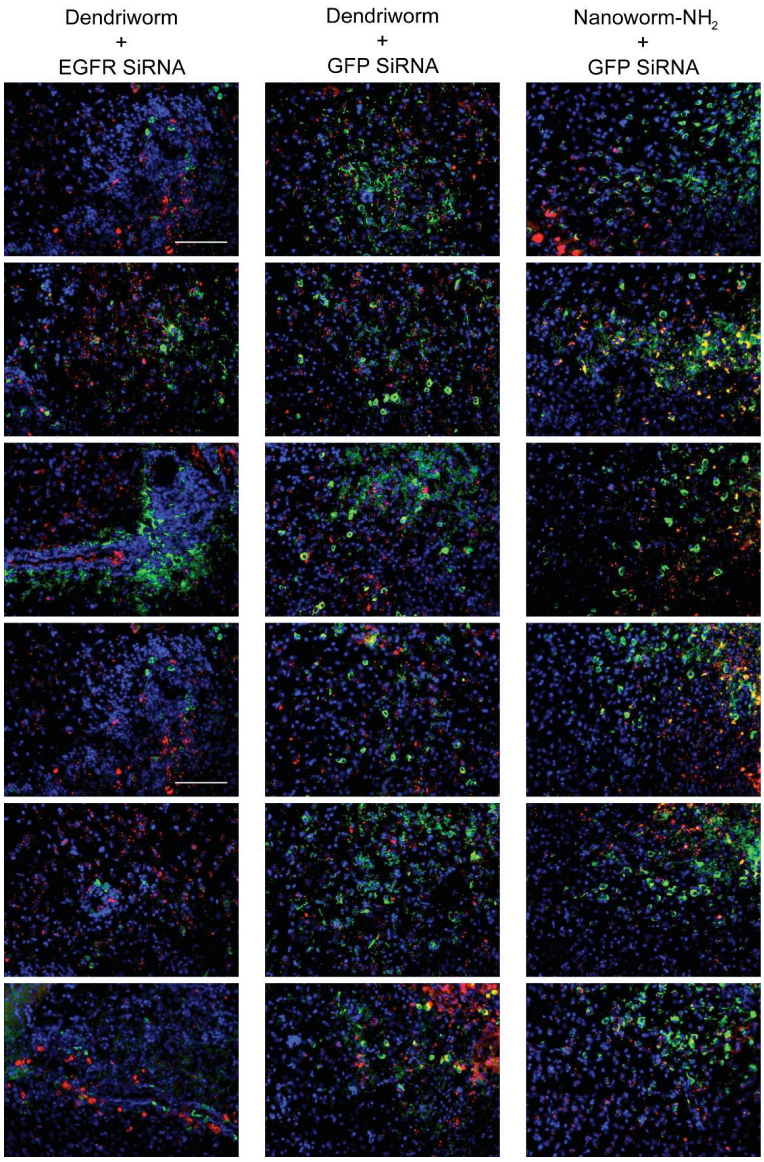

Figure S8. Histology data from all six sections imaged for various nanoparticle + siRNA formulations used in the *in vivo* studies

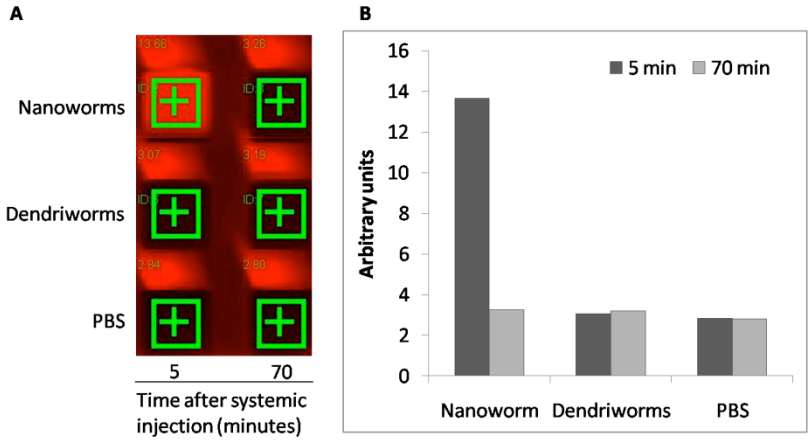

Figure S9. Circulation time of dendriworms and nanoworms. A: Nanoworms or dendriworms (12 ug iron) were injected into the tail vein of Swiss Webster mice and blood was drawn at 5 min or 70 min after injection. While nanoworms were present in blood at 5 min post injection, dendriworms were cleared in under 5 min. B: Quantification of data obtained via infrared imaging of the samples.